Research Paper

Low Voltage Ride-Through Improvement of a Two-Stage Grid-Connected Photovoltaic System by Using an Optimized SPWM Technique

Alireza Azamian [1] , *Behrooz Rezaeealam* [1, *] , *Teymoor Ghanbari* [2] , and *Esmaeel Rokrok* [1]

[1]*Electrical Engineering Department, Lorestan University, Khorramabad, Iran.*
[2]*School of Advanced Technologies, Shiraz University, Shiraz, Iran.*

Abstract— *Due to the increasing use of solar power plants as clean sources, their protection is vital to having desirable interaction with the main grids. This paper proposes a zero-sequence injection sinusoidal pulse-width modulation (ZSI_SPWM) technique for a three-level neutral point clamped (NPC) inverter for a photovoltaic (PV) system connected to the unbalanced three-phase grid. The proposed modulation technique injects the zero-sequence components to the grid as one of the SPWM reference signals, thereby significantly reducing the DC-link voltage oscillations and improve the low voltage ride-through (LVRT) condition. Also, this paper suggests optimal Sugeno fuzzy logic controllers (FLCs) to improve the LVRT capability of a PV connected to an unbalanced main grid, in which FLC rules are designed using the meta-heuristic krill Herding algorithm (KHA). The Gaussian memberships of Sugeno FLCs and proportional-integral (PI) parameters are optimally derived and used for reactive power and ZSI_SPWM simultaneously. The three-phase grid-connected PV system's power quality is improved by minimizing the multi-objective fitness function with multi-dimensionality. The proposed strategy reduces the DC side voltage oscillation, decreases the total harmonic distortion (THD), and stabilizes the output current, voltage, and flowing power. In this article, a dual second-order generalized integrator frequency locked loop (DSOGI-FLL) is used for better synchronizing the inverter with the grid during asymmetric faults due to its noise attenuation and frequency adaptability characteristics. The performance of the proposed approach is confirmed using simulations in different scenarios in the MATLAB/Simulink environment.*

Keywords—Fuzzy-Krill herding algorithm, low voltage ride-through, proportional-integral-Krill herding algorithm, zero sequence current control.

NOMENCLATURE

i_0^* Zero-sequence reference current
I_{max} The circuit maximum tolerable passing current (A)
V_0^* Zero-sequence reference voltage
i_{dc} The current of the DC link
P^* The active reference power(W)
Q^* The reactive reference power(var)
V_{pcc} The voltage of the inverter to the PCC(V)
(THD)   Total harmonic distortion
DSOGI_FLL   Dual second-order generalized integrator frequency locked loop
FLC   Fuzzy logic controller
KHA   Krill Herding algorithm
LVRT   Low voltage ride-through
NPC   Neutral point clamped
PCC   Point of common coupling
SCR   Short-circuit ratio
ZSI_SPWM   Zero-sequence injection sinusoidal pulse-width modulation

1. INTRODUCTION

Rapid developments in electricity grids, increasing energy demand, and environmental problems have increased the need for electricity generation by solar power stations [1, 2]. The increase in the production of solar power plants has led to an increase in the level of grid short-circuit current and an increase in the limits of infrastructure and switchboards [3, 4]. Upon a fault occurrence, in addition to compensating for the voltage drop caused by the fault in the grid, the power and current oscillations that reduce the capacitors' durability and damage the semiconductor components must also be reduced [5, 6]. One of the critical considerations in protecting solar power stations is the proper selection of power electronic interfaces (PEI). The three-level inverter has received much attention in recent years. The NPC inverter topology is the most common three-level inverter used in renewable energy. A suitable modulation strategy is very important for improving the voltage oscillations of the dividing capacitor in the three-level NPC inverter. In [7], a novel PWM strategy has been proposed for three-level NPC, in which PWM sequences are obtained by comparing a single carrier wave with dual modulation waves. The proposed PWM strategy increases switching losses, which limits its application. In [8], a method of constant voltage injection into SPWM has been introduced based on the maximum and minimum phase voltages of a five-phase, three-level inverter with a neutral

point. The effectiveness of the stated method was investigated for different load conditions; however, it was not checked for faults in the main grid connected to PV.

In addition to choosing the appropriate modulation for switching, optimizing the controllers has a significant effect on reducing oscillations. A strategy to apply fuzzy and proportional-integral (PI) controllers with optimized rules and parameters. Fuzzy rules and PI controller coefficients should be optimally selected to ensure correct operation and robust control of the system despite insufficient system information [9]. Various intelligent algorithms have been recently proposed to improve the performance of conventional LVRT methods.

In [10], a fuzzy-based LVRT control has been proposed that produces a ripple-less output; however, it does not limit dc link voltage ripples well. In [11], a probabilistic wavelet fuzzy-based neural network controller has been proposed for reactive power control during grid faults that has a fast response and improves settling time, but it is ineffective in improving DC link voltage oscillations. In [12], it has been proposed to use a gray wolf optimizer (GWO) in a three-phase 5MW grid-connected PV system to improve the LVRT, in which the PI controller parameters are tuned by GWO (GWO-PI). The number of iterations required to reach the optimal value of the fitness function with this method is high. Also, the performance of this method for asymmetric faults has not been investigated. In [13], the PI controller parameters were tuned by the PSO (PSO-PI) method, which includes many iterations. In [14], a fuzzy maximum power point tracking (MPPT) controller is proposed for various environmental conditions with a modified Krill Herding (MKH) algorithm. In [15], an optimal sliding mode controller (SMC) with -modified krill Herd (MKH) algorithm for MPPT in PV considering various weather conditions is proposed. In [16], to improve the performance of the grid-connected wind power plant, the parameters of the PI controller have been tuned using the ant lion optimizer (ALO) algorithm. Tuning the coefficients of the PI controller with the ALO algorithm has improved the LVRT performance and tracked the maximum power point. To improve the dynamic stability of the system and ensure LVRT capability, a cut-out strategy has been proposed in [17] for doubly-fed induction generator (DFIG) wind turbines so that reactive power is controlled with asynchronous load reduction. In [18], a control method based on multimode inverter control with fault tolerance according to grid code has been proposed. In this method, according to the severity of the grid faults, active and reactive powers are injected into the grid based on the grid code. In the proposed strategy, the exit of PV is prevented during the fault, and also the fuzzy controller has been used to control the maximum PV output power. Disadvantages of the proposed control method include the lack of control of the zero-sequence current and the unchanged coefficients of the controllers used in different conditions, which cause a lack of accurate control of grid fluctuations. In [19], a coordinated control strategy of active and reactive power based on the DC and AC side voltages has been proposed to adjust the medium voltage distribution grid with PV generation. According to the results obtained from the analysis, the flexible design of the controller ensures grid's stability during the fault, though it employs PI controllers with fixed coefficients and control strategy without considering the zero-sequence current. The approach presented in [20] is based on the Marine Predator Algorithm for obtaining the optimized PI controller parameters, to improve the LVRT in terms of overshoot, undershoot, settling time and steady-state response of the system. This study only takes into account the system conditions in three-phase faults without considering zero sequence. In [21], a new single-phase transformerless grid-connected PV inverter is presented. The design of the proposed structure is based on keeping the common mode voltage constant in order to suppress the leakage current and to provide the ability to inject reactive power during the fault in the network. In this article, the effect of zero sequence current is not considered. Also, the control method is based on the new inverter structure.

According to the above discussions, the mentioned methods have limitations in terms of less robustness and longer calculation times than KHA, given the complexity of the studied system. In addition, they have not sufficiently discussed the effects of inverter performance optimization to improve power quality and reduce DC link voltage oscillations under fault conditions in the three-phase grid.

As it is clear from the mentioned studies, the KHA algorithm can achieve an optimal solution in a shorter computing time than the other methods. It has also been shown in the studies mentioned above, that optimization algorithms play an important role in achieving the optimal design of PI controllers for power converters in PV systems.

Therefore, the proposed strategy in the present study uses the KHA algorithm for the optimal design of fuzzy rules and PI controller parameters. So, the purpose is to obtain the optimal 49 fuzzy rules for active power control and optimal values for reactive power and DC link voltage (to modulate ZSI_SPWM) PI controllers in a way that improves the power quality and stability of the PV system connected to the three-phase unbalanced grid. Simulation of a grid-connected three-phase PV system is done using MATLAB/Simulink. The simulation results show the effect of the proposed ZSI_SPWM modulation on reducing the DC link voltage oscillations, and also demonstrate the superiority of the fuzzy and PI controllers optimized with KHA over the fuzzy and PI controllers without optimization techniques.

The analysis of the subject system and the proposed LVRT control strategy are presented in Section 2, and the simulation results are discussed in Section 3.

2. THE LVRT CONTROL STRATEGY

The purpose of the proposed control strategy is to meet the requirements of LVRT and reduce the fluctuations of both DC and AC parts during the fault in the studied system. The proposed strategy consists of three parts. In the first part, the oscillations on the DC side caused by the zero-sequence current are reduced by presenting a new SPWM modulation method. In previous works, the effect of zero-sequence current on grid fluctuations during LVRT was less investigated. In this article, this issue is specifically investigated. In the second part, using optimized fuzzy and PI controllers, the reference values for the new SPWM modulation are calculated. By using these intelligent controllers, in addition to reducing power oscillations, the response speed of the system also increases. In previous articles, the controlling parameters have been derived experimentally, while in the current article, the controller parameters are obtained using the intelligent algorithm. In the third part, according to the grid codes, the necessary reactive power is injected into the grid to prevent the voltage drop caused by the faults. In previous LVRT studies, little attention has been paid to the reduction of oscillations caused by zero sequences in grid-connected PV. The proposed control strategy increases the lifetime of DC capacitors and PEI by reducing the AC and DC sides' fluctuations in the system, as the three-phase impedances are unbalanced in the grid side. In the system under study, a three-level NPC inverter is employed to improve output voltage quality and reduce voltage oscillations [22]. A three-level interleaved boost DC converter is also used to amplify the PV output voltage [23].

2.1. The proposed zero sequence injection SPWM (ZSI_SPWM) technique

In this study, the reduction of oscillations caused by zero sequence simultaneously at two neutral points (NP) on the DC side and PCC on the AC side in LVRT has been investigated for the first time. In [24, 25], new spatial vector pulse width modulation (SVPWM) methods are presented to reduce oscillations at the two mentioned points. In these studies, the fluctuation caused by the zero-sequence current passing through the common ground on

Table 1. Three-level NPC inverter output voltages.

Switches	Status	Inverter output voltage
S_{a1}, S_{a2}	ON	$+V_{dc}/2$
S_{a2}, S_{a3}	ON	0
S_{a3}, S_{a4}	ON	$-V_{dc}/2$

both the AC and DC sides is not taken into account. Also, the SVPWM method has more complexity and switching losses than the SPWM method. For this purpose, in the present study, by presenting the new SPWM method, the fluctuations caused by the zero-sequence current due to the phase impedance imbalance and unbalanced faults in the AC grid are reduced simultaneously on both the DC and AC sides. In the studied system, the impedance inequality of the phases and the occurrence of an asymmetric fault in the grid cause the zero-sequence current to flow from the common ground of the Wye-Grounded transformer and NPC, as shown in Fig. 1. This problem causes damage to the NPC inverter input capacitor and reduces its durability. Some methods are used to improve system performance against oscillations caused by zero sequences. To this end, a method of zero-sequence current injection into SPWM is proposed to generate the proper reference switching signal for a three-level NPC inverter. The relationship between the switching function and the output voltage of the NPC inverter is tabulated in Table 1.

As the capacitances C_u and C_L in Fig. 1 are equal, then:

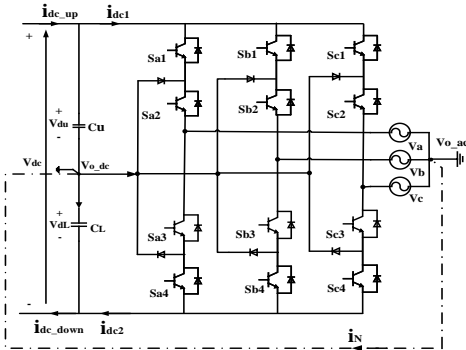$$i_{dc\_up} = -i_{dc\_down} \tag{1}$$
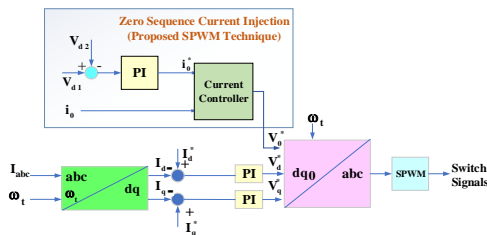

Fig. 1. Ground current between AC and DC sides.

Fig. 2. Zero-sequence injection for the inverter switching.

i_{dc_up} and $-i_{dc\_down}$ are shown in Fig. 1.

Eqs. (2) and (3) are related to capacitors at the input of the inverter:

$$C_u dV_{dcu}/dt = i_{dc\_up} - i_{dc1} \tag{2}$$

$$C_L dV_{dcL}/dt = i_{dc\_down} - i_{dc2} \tag{3}$$

That is:

$$Cd(V_{du} - V_{dL})/dt = i_N \tag{4}$$

Where $C_u = C_L = C$. i_N is the current flowing between two earths on both sides of the system.

Eq. (4) is rewritten as:

$$Cd(V_{du} - V_{dL})/dt = 3i_0 \tag{5}$$

Here i_0 is grid zero-sequence current and, i_N is given by:

$$i_N = i_a + i_b + i_c \tag{6}$$

i_a, i_b and i_c are the currents of each phase.

The current of the DC link (i_{dc}) for the NPC three-level inverter, which includes the zero-sequence component, can be written in the following form:

$$i_{dc} = \frac{1}{2}\left[f_a(t)i_a(t) + f_b(t)i_b(t) + f_c(t)i_c(t)\right] \tag{7}$$

Where f_i (i represents each phase) is the modulating signal and i_i is the current of the intended phase.

By separating the zero sequences of i_i and f_i:

$$i_i = i_i' + i_0 \tag{8}$$

$$f_i = f_i' + f_0 \tag{9}$$

Then, substituting Eqs. (8) and (9) into Eq. (7):

$$i_{dc} = \frac{1}{2}\left[f_a'(t)i_a'(t) + f_b'(t)i_b'(t) + f_c'(t)i_c'(t)\right] + 3f_0.i_0 \tag{10}$$

In the case of zero sequences, $3\,f_0.i_0$ would be a double-frequency term, which causes an oscillation in the DC link. In the proposed SPWM technique to reduce the zero-sequence current oscillations, the zero-sequence value is not always constant and equal to zero. In the proposed method, the zero-sequence reference i_0^* is calculated according to the voltage difference between the inverter input capacitors and the zero-sequence current of the system as shown in Fig. 2:

$$i_0^* = P_{Pdc}(V_{du} - V_{dL}) + \int I_{Idc}(V_{du} - V_{dL})dt \tag{11}$$

Where, P_{Pdc} and I_{Idc} are the proportional and integrator coefficients of the PI controller shown in Fig. 2, respectively. In the proposed ZSI_SPWM technique, the reference zero-sequence voltage (V_0^*) is derived as the output of the current controller:

$$V_0^* = P_{Pcc}(i_0^* - i_0) + \int I_{Icc}(i_0^* - i_0)dt \tag{12}$$

Where, P_{Pcc} and I_{Icc} are the proportional and integrator coefficients of the corresponding PI controller, respectively, as depicted in Fig. 2. These PI coefficients are calculated using the intelligent algorithm to improve the system performance. The method of calculating these coefficients is explained in the next section. Also, DSOGI_FLL, which is appropriate for high-level harmonics elimination in three-phase systems, has separated the sequences [26].

2.2. Tuning fuzzy rules and PI controller parameters by Krill Herd algorithm (Fuzzy_KHA & PI_KHA)

One of the decisive parameters for system oscillations is the short-circuit ratio (SCR), which is calculated as [27]:

$$SCR = \frac{S_{AC\_Grid}}{S_{Rate}} \qquad (13)$$

Where S_{AC} and S_{Rate} are the short-circuit capacity of the AC system and the rated power generated by the PV system, respectively. According to the standard for distributed energy sources, the value of SCR must be higher than 20 for a PV system connected to a grid through an inverter [22] to have stable operation. In the studied PV system connected to a three-phase grid with the peak phase voltage of 155 V, grid impedance $(1.9032 + 7.9089j)\Omega$ and the rated power of 1.7kW, the SCR is computed as:

$$SCR = \frac{155 * 155}{1.7kW * |1.9032 + 7.9089j|\,\Omega} = 1.74$$

That is lower than 20, leading to stability problems and power quality requirements [28]. In addition, compliance with LVRT requirements causes oscillations and even instability in the output active and reactive powers of the inverter [29]. Therefore, advanced controllers are required to improve the stability of grid-connected PV power plants, especially for the case of LVRT under grid faults.

Advanced nonlinear control methods such as sliding model [30] and back-stepping [31] methods and similar controllers have computational complexity. Also, these methods require the system state equations. According to the cases mentioned, it is necessary to use control methods with less computational complexity and that are robust to the system oscillations. For this purpose, in this study, fuzzy and PI controllers with rules and coefficients optimized with meta-heuristic intelligent algorithms are used. Traditional fuzzy and PI controllers are very popular. But if fuzzy rules and the proportional (P) and integral (I) control parameters are not selected correctly, these controllers do not perform properly in abnormal conditions, such as faults. In this process, for the proper performance of the fuzzy and PI controllers in all conditions, fuzzy rules and PI controller parameters are determined using KHA.

The KHA is based on the behaviour of krill to find food. This algorithm was presented by Gandomi and Alavi in 2012 to optimize the mathematical model [32]. In the KHA, the shortest distance between each krill and food and the distance to the concentrated population of krill Herds are considered fitness functions for the movement of krills. Fig. 3 shows the flowchart of the KHA algorithm, and its implementation steps are described as follows:

In Step 1.1, the algorithm parameters are defined, including the number of runs (NR), number of krill (NK), the maximum number of iterations (MI), crossover flag (C-flag), problem bounds including lower and upper bounds (LB, UB) (here, the basic rules of fuzzy controller and the upper and lower limits of PI controller parameters are determined), number parameters (NP), and scale factor (Dt).

Step 1.2: The parameters of the algorithm to change the positions of krill with respect to time (dX_j/dt) are defined:

$$dx_j/dt = N_j + F_j + D_j \qquad (14)$$

Where N_j, F_j and D_j are the induced motion, foraging motion, and physical diffusion, respectively. Here, the initial values of these parameters are set to zero.

Step 2: The initial positions of the krills are set randomly, which is the same as the basic fuzzy rules and the initial PI controller's parameters:

$$X_j = LB_j + (UB_j - LB_j) * rand()$$
$$j = 1, 2, ..., NP \qquad (15)$$

Step 3: In this step, we calculate the fitness function according to the number of krill and also to the positions determined in step 2.

Fitness function: In order to properly operate the PV connected to three-phase unbalanced grid in normal conditions and during the fault, 49 fuzzy rules and six parameters of PI controllers are considered in Fig. 4-b. These parameters include active power fuzzy controllers, reactive power and DC-side voltage PI controllers. The ITAE objective fitness function for KHA optimization is considered as:

$$\min F(x) = w_1 \int_0^{T_{\max}} t\,|e_P(t)|dt + w_2 \int_0^{T_{\max}} t\,|e_Q(t)|dt +$$
$$w_3 \int_0^{T_{\max}} t\,|e_Z(t)|dt + w_4 \int_0^{T_{\max}} THD_V dt \qquad (16)$$

Where e is the error, W_{1-4} are the weight coefficients, $T_{\max}$ is the maximum time, and THD_V is the THD of output voltage. In this objective function, in addition to reducing the error of reactive and active powers and the voltage difference of the capacitors on the DC side of the inverter, because the zero-sequence current in the circuit causes this difference, the THD reduction is also taken into account.

Step 4: In this step, according to the previous steps, we update the fuzzy rules and the values of the PI parameters or the position of the krill Eq. (14) according to the fitness function Eq. (16). In this step, genetic operators are also induced to KHA through crossover and mutation.

Step 5: In this step, the best fuzzy rules and the value of PI controller parameters are determined using the KHA algorithm.

2.3. Strengthening the positive sequence

Upon a short circuit fault occurrence in the AC grid, the voltage drop occurs due to the increase in grid current [33, 34]. By deactivating the MPPT mode in PV, a part of the injected active power is allocated to the reactive power. Reactive power injection, according to the E.ON standard Eq. (17), compensates the voltage drop of AC grid-connected to PV during the fault [35]:

$$I^*_{q(pu)} = \begin{cases} 0 & V_{drp} < 0.1 \\ 2 * V_{drp} & 0.1 < V_{drp} < \frac{1}{2} \\ 1 & V_{drp} > \frac{1}{2} \end{cases} \qquad (17)$$

Here $V_{drp(pu)}$ is:

$$V_{drp(pu)} = 1 - |V^+_{rms}|/V_{base} \qquad (18)$$

Here V_{base} is the rated grid voltage. The $|V^+_{rms}|$ is calculated by Eq. (19):

$$|V^+_{rms}| = \sqrt{\frac{1}{3}(V^{+2}_{pcca} + V^{+2}_{pccb} + V^{+2}_{pccc})} \qquad (19)$$

Where $V_{pcc(x)}$ is the point of common coupling (PCC) voltage of the grid and the inverter. In unbalanced conditions, for each phase in PCC, the value of positive sequence voltage is calculated as:

$$\begin{bmatrix} V^+_{pcca} \\ V^+_{pccb} \\ V^+_{pccc} \end{bmatrix} = \frac{1}{3} \begin{bmatrix} 1 & a & a^2 \\ a^2 & 1 & a \\ a & a^2 & 1 \end{bmatrix} \begin{bmatrix} V_{pcca} \\ V_{pccb} \\ V_{pccc} \end{bmatrix} =$$
$$\sqrt{2}\,|V^+_{rms}| \begin{bmatrix} \sin(\theta_i) \\ \sin(\theta_i - \frac{2\pi}{3}) \\ \sin(\theta_i + \frac{2\pi}{3}) \end{bmatrix} \qquad (20)$$
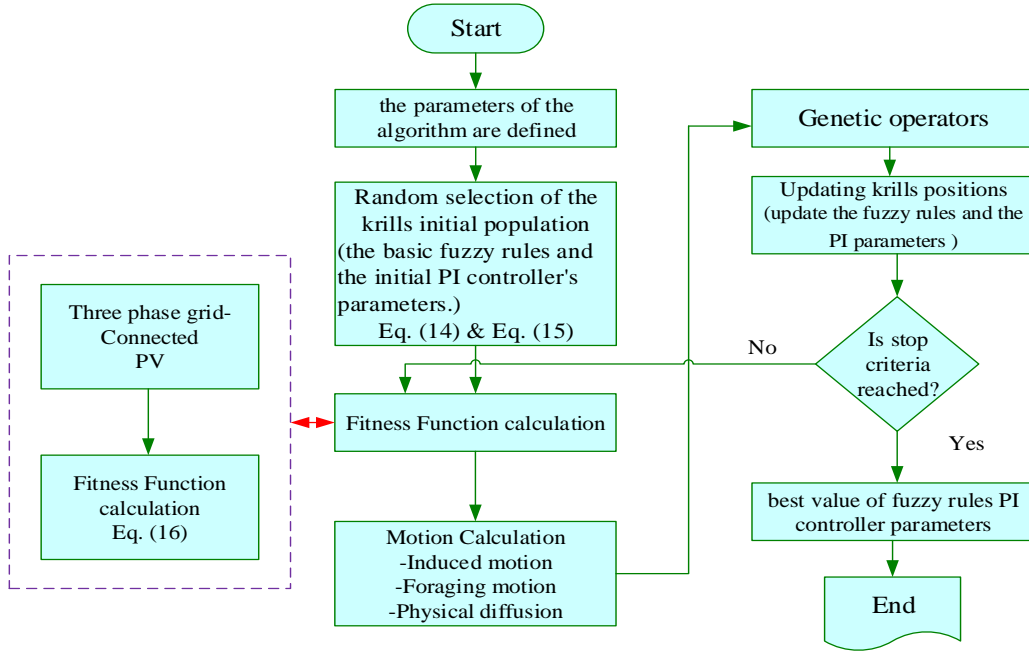
Fig. 3. Optimization flowchart with KHA algorithm.

Table 2. The solar power plant specifications.

Parameter	Value
Maximum power (W)	210W
Number of series modules	1
Short-circuit current I_{sc} (A)	8A
Number of parallel string	10
Open circuit voltage V_{oc} (V)	40V

Table 3. AC grid specifications (Fig. 4-a).

Parameter	Value
Grid line-line voltage (RMS)	190V
Generated active power	1.7kW
Rated current amplitude	4.5A
Inductance side of the LCL filter	26.1mH
Switching frequency	20kHZ
LCL filter capacitance (Grid side)	2.6mF
DC-link capacitor	3760mF
Phase impedance b	$(1.8584 + 8.2242j)\Omega$
Nominal grid frequency	50HZ
Phase impedance a	$(1.87921 + 8.5432j)\Omega$
LCL filter inductance (Inverter side)	1.6mH
Phase impedance c	$(1.9032 + 7.9089j)\Omega$

Where $a = e^{j2\pi/3}$.

The reactive reference power Q^* and active reference power P^* are calculated as follows:

$$Q^* = |S|\, I^*_{vr(pu)} \tag{21}$$

$$P^* = |S|\, \sqrt{1 - I^{*2}_{vr(pu)}} \tag{22}$$

Where $I^*_{vr(pu)} = I^*_{q(pu)}$ is calculated through Eq. (17).
The maximum apparent transferable power is calculated as:

$$|S| = (|V_{pcca}|_{rms} + |V_{pccb}|_{rms} + |V_{pccc}|_{rms})I_{\max} \tag{23}$$

That:

$$I_{\max} = \cfrac{1}{\sqrt{\frac{(V^+)^2 - 2V^+V^- \min(\Re) + (V^-)^2}{(V^+)^2}\left((I^+_p)^2 + (I^+_q)^2\right)}} \tag{24}$$

Parameter $\Re$ in Eq. (24) is given by:

$$\Re = (\cos(\theta) \quad \cos(\theta - \frac{2\pi}{3}) \quad \cos(\theta + \frac{2\pi}{3})) \tag{25}$$

$$I^+_p = \frac{2}{3}(V^+ \big/ (V^+)^2 - (V^-)^2)P^* \tag{26}$$

The parameter I^+_q is calculated through Eq. (17).

3. SIMULATION RESULT

The system under study in Fig. 4 consists of a three-phase grid, which is supplied by a PV with the characteristics of Table 2. In the PV system, a three-level boost interleaved converter is used to boost the DC voltage, and an NPC inverter is used to connect the PV system to the AC grid. The characteristics of the studied system (Fig. 4-a) are described in Table 3.

The proposed control approach in Fig. 4-b is simulated in the MATLAB/Simulink software. The better performance of Fuzzy-KHA is revealed compared to the case where the fuzzy controller parameters are calculated by the trial-and-error method.

Simulations are performed for three scenarios: (1) At first, inverter switching is done by the conventional SPWM method through the control strategy, and zero-sequence is not injected ($V^*_0 = 0$). Then, according to the proposed strategy, V^*_0 is calculated as shown in Fig. 2, which is equal to the value of the zero-sequence voltage shown in Fig. 4-a. (2) Under normal operating conditions, an unbalanced three-phase grid is connected to the PV system. (3) A single-phase-to-ground fault is modeled with a duration of 50ms on the grid side.

In this study, triangular membership functions (MF), including overlap, are used, they are composed of seven linguistic variables as follows: Negative big (NB), negative (N), negative small (NS),
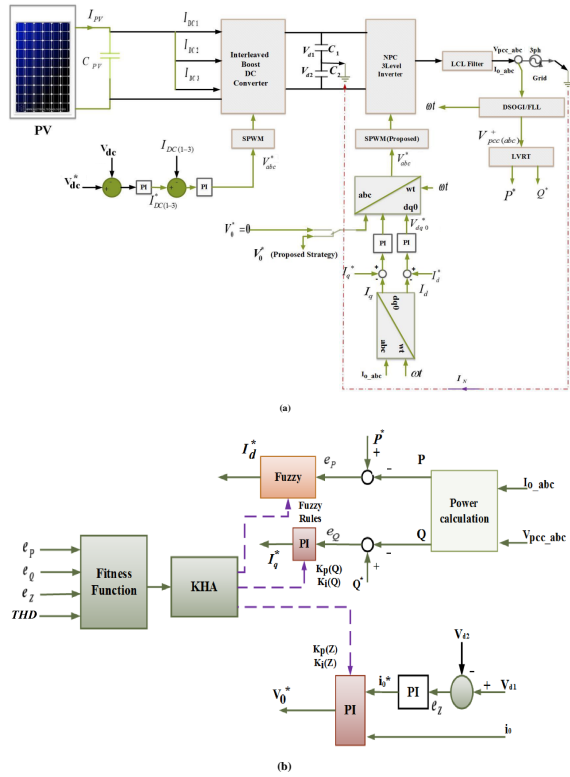
Fig. 4. The system block diagram: (a) PV system with three-phase grid; (b) The proposed strategies of PI-KHA and fuzzy-KHA.

Table 4. The FLC rules.

$\Delta(eP)^{eP}$	NB	N	NS	Z	PS	P	PB
NB	Z	PS	P	P	PB	PB	PB
N	PS	P	P	PB	PB	PB	P
NS	P	P	PB	PB	PB	P	PS
Z	P	PB	PB	PB	P	PS	PS
PS	PB	PB	P	P	PS	PS	Z
P	PB	PB	PS	PS	PS	Z	Z
PB	PB	P	PS	PS	Z	Z	Z
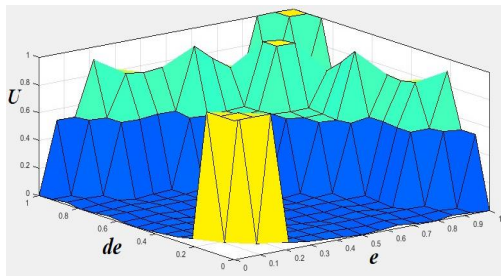
Fig. 5. FLC-KHA rules.

zero (Z), and positive small (PS), positive (P), and PB (positive big), respectively. The forty-nine fuzzy rules are presented in Table

Table 5. PI parameter calculation.

Parameter/ Method	Trial-and-error	KHA
Kp(Q)	0.3	0.0108
Ki(Q)	1.33	0.8345
Kp(Z)	0.76	0.1375
Ki(Z)	1.4	0.7931
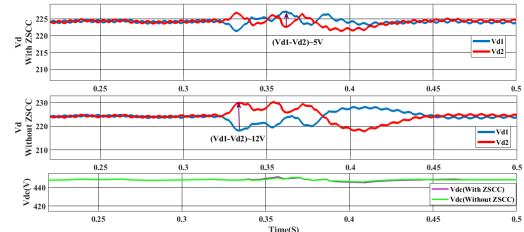
Fig. 6. DC side voltage.
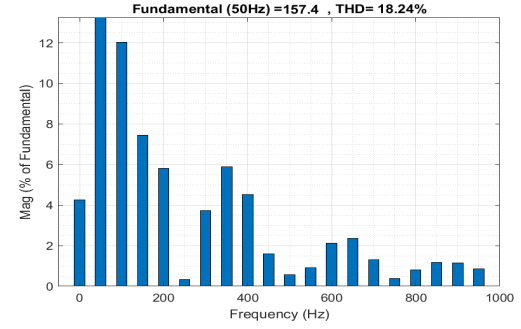
Fig. 7. Grid voltage harmonic coefficients with fuzzy controller.
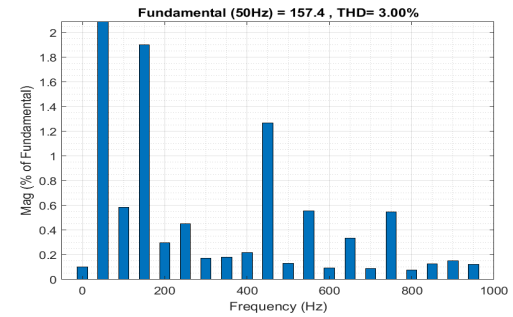
Fig. 8. Grid voltage harmonic coefficients with fuzzy-KHA controller.
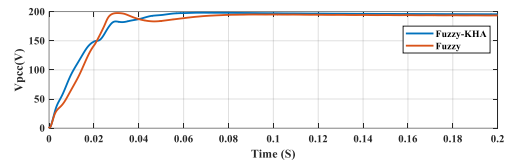

Fig. 9. Comparison of RMS voltage in PCC of the three-phase grid connected to PV normal condition.
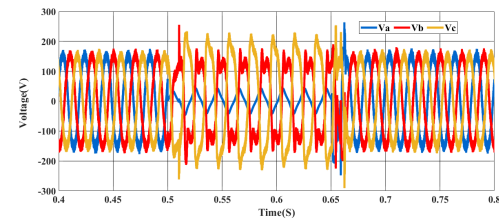

Fig. 10. Grid voltage with fuzzy controller.

4. In Table 4, (eP) is the active power error and $\Delta(eP)$ the change of the active power error. If the fuzzy rules are changed by KHA, the new rules are changed as shown in Fig. 5.

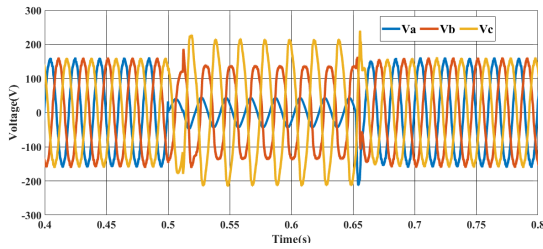Table 5 shows the parameters of the PI-KHA controllers.

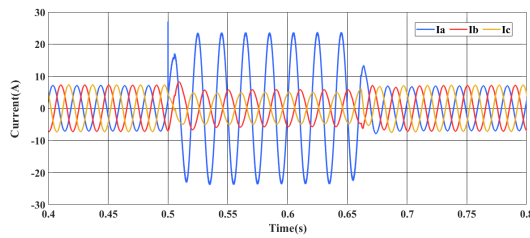Fig. 11. Grid voltage with fuzzy-KHA controller.

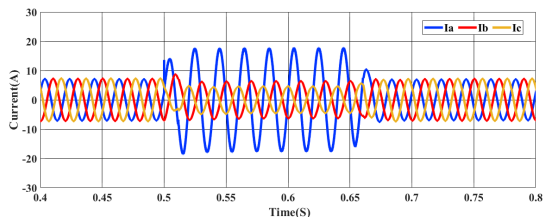Fig. 12. Grid current with fuzzy controller.

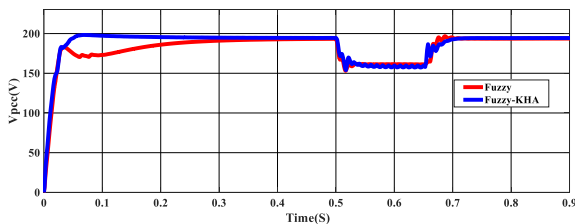Fig. 13. Grid current with fuzzy-KHA controller.

Fig. 14. Comparison of RMS voltage in PCC of the three-phase grid connected to PV single-phase to ground.
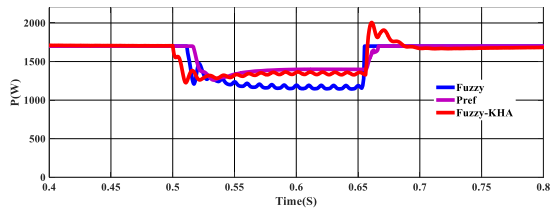

Fig. 15. Active powers injected into the grid.

PI-KHA controller parameters and fuzzy-KHA rules with KHA have reached the best solution with very high speed.

3.1. Investigating the effect of zero-sequence injection

One of the purposes of this study is to investigate how the injection of zero-sequence current into SPWM influences the system behavior under normal and fault operating conditions. As mentioned, the DC and AC parts are connected to each
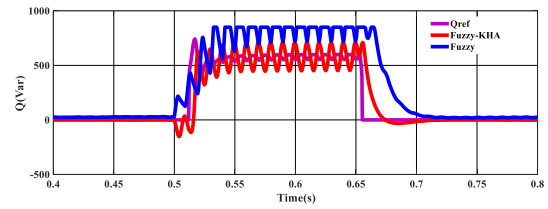

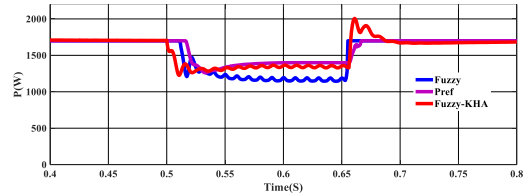Fig. 16. Reactive powers injected into the grid.

Fig. 17. Comparison of RMS voltage in PCC of the three-phase grid connected to PV (2 phase fault).
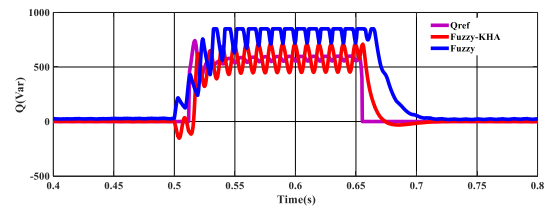

Fig. 18. Grid current with fuzzy controller (2 phase fault).

other through the ground, and the main grid is supposed to be unbalanced. Zero-sequence current flows between these two parts, which leads to unbalanced voltages across the capacitors and the NPC inverter. It is intended to minimize the difference between the voltages of the capacitors by considering the nonzero constant value for zero sequence current in SPWM using the zero-sequence current controller (ZSCC) illustrated in Fig. 2. As shown in Fig. 6, in the event of a single-phase-to-ground fault, which causes more zero-sequence current to flow in the circuit, the difference between capacitors' voltages becomes up to $\sim 12V$ in the absence of zero-sequence injection, while it is reduced down to less than 5V with the employed zero-sequence injection. In other words, by injecting the zero-sequence current into SPWM, the spread of oscillation from the DC side of the inverter to its AC part is largely prevented.

3.2. Case 2: Normal condition

Fig. 7 shows the voltage THD of 18.24% for the three-phase grid when the fuzzy controller rules are obtained by trial and error. Fig. 8 shows the voltage THD of 3% for the three-phase grid when the fuzzy controller coefficients are obtained with KHA. As shown in Figs. 7 and 8, for the case of obtaining conventional fuzzy rules, the THD value is larger than the one achieved by fuzzy rules derived from KHA. As shown in Fig. 9, for the case of conventional fuzzy rules, the peak value of the RMS voltage in PCC is 190V, and more oscillations happen to reach steady state compared to the case with fuzzy rules from KHA (fuzzy-KHA). Also, the system with the fuzzy controller has overshoot and initial undershoot, while the damping speed of the system has been improved with the fuzzy-KHA controller.

Table 6. Comparison of the proposed method.

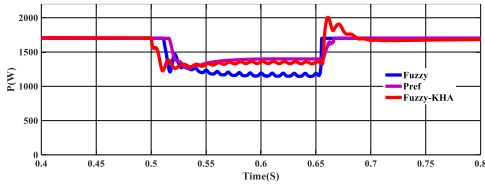| Method \ Result	Transient response time (Sec)	The number of iterations	THD(%)	Asymmetric fault checking	PV connection to asymmetric three-phase grid	Zero sequence control
PI-GWO [12]	0.13	10	4.57	×	×	×
PI-PSO [13]	0.185	40	2.72	✓	×	×
PI-KHA	0.18	4	2.04	✓	✓	✓

Fig. 19. Grid current with fuzzy-KHA controller (2 phase fault).
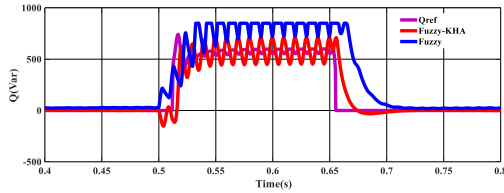

Fig. 20. Comparison of RMS voltage in PCC of the three-phase grid connected to PV (3 phase fault).
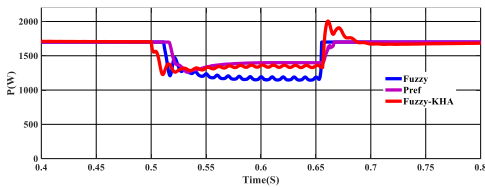

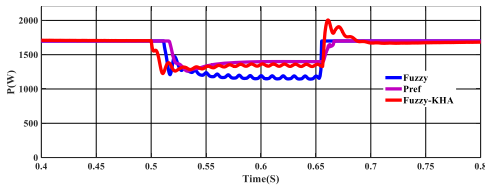Fig. 21. Grid current with fuzzy controller (3 phase fault).

Fig. 22. Grid current with fuzzy-KHA controller (3 phase fault).

3.3. Case 3: Single-phase-to-ground fault in the three-phase grid

As shown in Figs. 10–13, the fuzzy-KHA controller improves the stability of the system as the transient time and oscillations are reduced during the single-phase-to-ground fault in the three-phase grid in comparison with the results obtained from the fuzzy controller. As shown in Figs. 12 and 13, the peak current with the fuzzy controller is 30A, while this value is less than 20A for the fuzzy-KHA controller.

Fig. 14 shows the value of the RMS voltage in PCC for both fuzzy controllers. The superiority of the fuzzy-KHA controller is evident in terms of better stability and suppressed oscillations during the fault period.

The active and reactive power injected into the grid with fuzzy and fuzzy-KHA controllers are shown in Figs. 15 and 16, respectively. The latter causes fewer oscillations in power and better performance during fault times.

3.4. Case 4: Two-phase fault in the three-phase grid

As shown in Figs. 17–19, the fuzzy-KHA controller improves the stability of the system as the transient time becomes shorter, and also the voltage fluctuation is reduced by about 10 volts during the two-phase fault in the three-phase grid in comparison with the results obtained from the fuzzy controller.

Fig. 17 shows the value of the RMS voltage in PCC for both fuzzy controllers. The superiority of the fuzzy-KHA controller is evident in terms of better stability and suppressed oscillations during the fault period.

3.5. Case 5: Three-phase fault in the three-phase grid

As shown in Figs. 20–22, the fuzzy-KHA controller improves the stability of the system, as well as oscillations are reduced during the three-phase fault in the three-phase grid in comparison with the results obtained from the fuzzy controller.

As shown in Fig. 20, the amount of voltage fluctuations with the fuzzy-KHA controller is 10 volts less than the one with the fuzzy controller. Also, the fuzzy-KHA controller shortens the time needed to reach the final response.

As mentioned in Introduction, in [12] a grey-wolf optimizer (GWO) has been employed to estimate the optimal coefficients of the PI controller and then to enhance the LVRT in a 5MW three-phase grid-connected PV system. Also, in [13] the particle swarm optimisation (PSO) technique has been implemented to tune the PI controller parameters for an inverter in a three-phase grid-connected PV system. It is of interest to compare the performance of the proposed method with the ones of [12] and [13], in terms of transient response time, the required number of iterations and THD that are briefly summarized in Table 6. It is seen that the proposed method provides an acceptable improvement in the performance of the system with a lower number of iterations.

4. CONCLUSION

The design and simulation of the proposed control strategy for controlling an unbalanced three-phase grid-connected PV system were presented. DC link voltage oscillations were significantly reduced, and also a 58% reduction in the voltage difference of the input DC link capacitors of the NPC inverter was achieved using the proposed ZSI_SPWM technique compared to conventional SPWM. In addition, the settling time of the input voltages was decreased by 33% as the KHA algorithm was used to obtain active power fuzzy controller rules, reactive power PI controller coefficients, and also PI controller coefficients in the proposed ZSI_SPWM method. The results showed that with the proposed optimized controllers, the voltage THD in PCC would be six times lower than that of the conventional controller. Also, the fuzzy-KHA controller caused a 67% reduction in the peak current due to the single-phase-to-ground fault, as well as the voltage fluctuation was reduced by about 10 volts during the two-phase and three-phase fault in the three-phase grid, in comparison with the fuzzy one. In previous works, the use of intelligent controllers has been less common, while in this research in addition to using the fuzzy controller, the parameters of the controllers have been tuned by KHA that requires a lower number of iterations in comparion with optimization algorithms of GWO and PSO.

REFERENCES

[1] M. B. Hayat, D. Ali, K. C. Monyake, L. Alagha, and N. Ahmed, "Solar energy—a look into power generation, challenges, and a solar-powered future," *Int. J. Energy Res.*, vol. 43, no. 3, pp. 1049–1067, 2019.

[2] J. Yu, H. B. Saydaliev, Z. Liu, R. Nazar, and S. Ali, "The asymmetric nexus of solar energy and environmental quality: Evidence from top-10 solar energy-consuming countries," *Energy*, vol. 247, p. 123381, 2022.

[3] K. Mahmoud and M. Lehtonen, "Comprehensive analytical expressions for assessing and maximizing technical benefits of photovoltaics to distribution systems," *IEEE Trans. Smart Grid*, vol. 12, no. 6, pp. 4938–4949, 2021.

[4] M. Hamedi, H. Shayeghi, S. Seyedshenava, A. Safari, A. Younesi, and N. Bizon, "Optimal multi-period planning of the distribution network in the presence of wide-spread penetration of small-scale solar resources," *IET Renewable Power Gener.*, vol. 17, no. 13, pp. 3386–3402, 2023.

[5] K. Matharani and H. Jariwala, "Stability analysis of microgrid with passive, active, and dynamic load," *J. Oper. Autom. Power Eng.*, vol. 11, no. 4, pp. 295–306, 2023.

[6] N. Jaalam, N. Rahim, A. Bakar, and B. Eid, "Strategy to enhance the low-voltage ride-through in photovoltaic system during multi-mode transition," *Solar Energy*, vol. 153, pp. 744–754, 2017.

[7] W. Jiang, X. Huang, J. Wang, J. Wang, and J. Li, "A carrier-based pwm strategy providing neutral-point voltage oscillation elimination for multi-phase neutral point clamped 3-level inverter," *IEEE Access*, vol. 7, pp. 124066–124076, 2019.

[8] C. Odeh, D. Kondratenko, A. Lewicki, and A. Jąderko, "Modified spwm technique with zero-sequence voltage injection for a five-phase, three-level npc inverter," *Energies*, vol. 14, no. 4, p. 1198, 2021.

[9] M. Regad, M. Helaimi, R. Taleb, H. Gabbar, and A. Othman, "Optimal frequency control in microgrid system using fractional order pid controller using krill herd algorithm," , no. 2 (eng), pp. 68–74, 2020.

[10] M. K. Hossain and M. H. Ali, "Fuzzy logic controlled power balancing for low voltage ride-through capability enhancement of large-scale grid-connected pv plants," in *2017 IEEE Texas Power Energy Conf.*, pp. 1–6, IEEE, 2017.

[11] F.-J. Lin, K.-C. Lu, T.-H. Ke, B.-H. Yang, and Y.-R. Chang, "Reactive power control of three-phase grid-connected pv system during grid faults using takagi–sugeno–kang probabilistic fuzzy neural network control," *IEEE Trans. Ind. Electr.*, vol. 62, no. 9, pp. 5516–5528, 2015.

[12] N. Jaalam, A. Ahmad, A. Khalid, R. Abdullah, N. Saad, S. Ghani, and L. Muhammad, "Low voltage ride through enhancement using grey wolf optimizer to reduce overshoot current in the grid-connected pv system," *Math. Probl. Eng.*, vol. 2022, no. 1, p. 3917775, 2022.

[13] M. Roslan, A. Q. Al-Shetwi, M. Hannan, P. Ker, and A. Zuhdi, "Particle swarm optimization algorithm-based pi inverter controller for a grid-connected pv system," *PLoS One*, vol. 15, no. 12, p. e0243581, 2020.

[14] Z. Hu, H. Norouzi, M. Jiang, S. Dadfar, and T. Kashiwagi, "Novel hybrid modified krill herd algorithm and fuzzy controller based mppt to optimally tune the member functions for pv system in the three-phase grid-connected mode," *ISA Trans.*, vol. 129, pp. 214–229, 2022.

[15] Z. M. Ali, N. V. Quynh, S. Dadfar, and H. Nakamura, "Variable step size perturb and observe mppt controller by applying θ-modified krill herd algorithm-sliding mode controller under partially shaded conditions," *J. Cleaner Prod.*, vol. 271, p. 122243, 2020.

[16] A. Lotfy Haridy, A.-A. Ali Mohamed Abdelbasset, A. Mohamed Hemeida, and Z. Mohamed Ali Elhalwany, "Optimum controller design using the ant lion optimizer for pmsg driven by wind energy," *J. Electr. Eng. Technol.*, vol. 16, pp. 367–380, 2021.

[17] A. Tan, Z. Tang, X. Sun, J. Zhong, H. Liao, and H. Fang, "A cut-out strategy for wind turbines that ensures low-voltage ride-through capability," *J. Electr. Eng. Technol.*, vol. 15, no. 4, pp. 1567–1575, 2020.

[18] C. Nithya and J. P. Roselyn, "Multimode inverter control strategy for lvrt and hvrt capability enhancement in grid connected solar pv system," *IEEE Access*, vol. 10, pp. 54899–54911, 2022.

[19] O. Alrumayh, K. Sayed, and A. Almutairi, "Lvrt and reactive power/voltage support of utility-scale pv power plants during disturbance conditions," *Energies*, vol. 16, no. 7, p. 3245, 2023.

[20] H. H. Ellithy, H. M. Hasanien, M. Alharbi, M. A. Sobhy, A. M. Taha, and M. A. Attia, "Marine predator algorithm-based optimal pi controllers for lvrt capability enhancement of grid-connected pv systems," *Biomimetics*, vol. 9, no. 2, p. 66, 2024.

[21] F. Mohammadi, J. Milimonfared, H. Rastegar, and M. Farhadi-Kangarlu, "Design of a single-phase transformerless grid-connected pv inverter considering reduced leakage current and lvrt grid codes," *J. Oper. Autom. Power Eng.*, vol. 9, no. 1, pp. 49–59, 2021.

[22] S. R. Mohapatra and V. Agarwal, "Model predictive control for flexible reduction of active power oscillation in grid-tied multilevel inverters under unbalanced and distorted microgrid conditions," *IEEE Trans. Ind. Appl.*, vol. 56, no. 2, pp. 1107–1115, 2019.

[23] S. Shabani, M. Delshad, and R. Sadeghi, "A soft switched non-isolated high step-up dc-dc converter with low number of auxiliary elements," *J. Intell. Proced. Electr. Technol.*, 2022.

[24] X. Li, X. Xing, C. Zhang, C. Qin, X. Liu, G. Zhang, and B. Duan, "Neutral-point voltage oscillation mitigation scheme for transformerless three-level pv inverter in lvrt operation with selective space vector modulation," *IEEE J. Emerging Sel. Top. Power Electron.*, vol. 10, no. 3, pp. 2776–2789, 2020.

[25] Y. Li, X. Yang, W. Chen, T. Liu, and F. Zhang, "Neutral-point voltage analysis and suppression for npc three-level photovoltaic converter in lvrt operation under imbalanced grid faults with selective hybrid svpwm strategy," *IEEE Trans. Power Electron.*, vol. 34, no. 2, pp. 1334–1355, 2018.

[26] B. Brahmbhatt and H. Chandwani, "Grid synchronization for three-phase grid-tied converter using decouple-second-order generalized integrator," in *Proc. Int. Conf. Int. Syst. Signal Process.: e-ISSP 2020*, pp. 347–359, Springer, 2022.

[27] D. G. Photovoltaics and E. Storage, "Ieee standard for interconnection and interoperability of distributed energy resources with associated electric power systems interfaces," *IEEE std*, vol. 1547, no. 1547, p. 2018, 2018.

[28] S. M. Alizadeh, C. Ozansoy, and A. Kalam, "Investigation into the impact of pcc parameters on voltage stability in a dfig wind farm," in *2017 Australas. Univ. Power Eng. Conf.*, pp. 1–6, IEEE, 2017.

[29] S. Mortazavian and Y. A.-R. I. Mohamed, "Dynamic analysis and improved lvrt performance of multiple dg units equipped with grid-support functions under unbalanced faults and weak grid conditions," *IEEE Trans. Power Electron.*, vol. 33, no. 10, pp. 9017–9032, 2017.

[30] Y. Li, Y. Lei, X. Lin, and Y. Zhu, "Research on the application of an smes based on sliding mode control to enhance the lvrt capability of a grid-connected pv system," *Electr. Power Components Syst.*, vol. 47, no. 9-10, pp. 914–926, 2019.

[31] M. Nadour, A. Essadki, and T. Nasser, "Improving low-voltage ride-through capability of a multimegawatt dfig based wind turbine under grid faults," *Prot. Control Mod. Power Syst.*, vol. 5, pp. 1–13, 2020.

[32] A. H. Gandomi and A. H. Alavi, "Krill herd: a new

bio-inspired optimization algorithm," *Commun. Nonlinear Sci. Numer. Simul.*, vol. 17, no. 12, pp. 4831–4845, 2012.

[33] S. Mashaly and M. H. Abdallah, "Low voltage ride through and fault ride through capability of 40kw pv model grid connected," in *2016 Saudi Arabia Smart Grid*, pp. 1–6, IEEE, 2016.

[34] L. Guan and J. Yao, "Dynamic stability improvement scheme for dual-sequence plls in vsc based renewable energy generation system during asymmetrical lvrt," *Int. J. Electr. Power Energy Syst.*, vol. 145, p. 108683, 2023.

[35] S. W. Ali, A. K. Verma, Y. Terriche, M. Sadiq, C.-L. Su, C.-H. Lee, and M. Elsisi, "Finite-control-set model predictive control for low-voltage-ride-through enhancement of pmsg based wind energy grid connection systems," *Math.*, vol. 10, no. 22, p. 4266, 2022.